

Galvanomagnetic Coefficients of Single-Crystal Tellurium*

ALLEN NUSSBAUM AND ROBERT J. HAGER
 Honeywell Research Center, Hopkins, Minnesota
 (Received May 3, 1961)

The twelve galvanomagnetic coefficients of tellurium crystals grown by the Czochralski method were measured over the temperature range 77°–300°K. The results of these measurements plus previous measurements at 4.2°K and a determination of the effect of pressure on one of the Hall coefficients are combined with symmetry characteristics to postulate an energy band structure. This structure differs from those previously proposed on the basis of tight-binding methods or by simple applications of group theory.

INTRODUCTION

TELLURIUM is an elemental semiconductor whose crystal symmetry is illustrated in Fig. 1. There is a threefold screw axis perpendicular to the plane of the paper and three twofold axes lying in this plane. This

anisotropic structure results in the necessity for measuring twelve coefficients to specify the galvanomagnetic tensor and the screw-axis makes the calculation of the energy-band structure a difficult task. The electrical and optical properties of tellurium grown by the Bridgman method have been extensively studied in the past,¹ but more recently, Czochralski-type crystals have become available²; such crystals are desirable for band-structure study, since they minimize effects due to imperfections. Roth³ has published curves of some of the galvanomagnetic coefficients as measured on a pulled crystal supplied by this laboratory, and curves for some additional

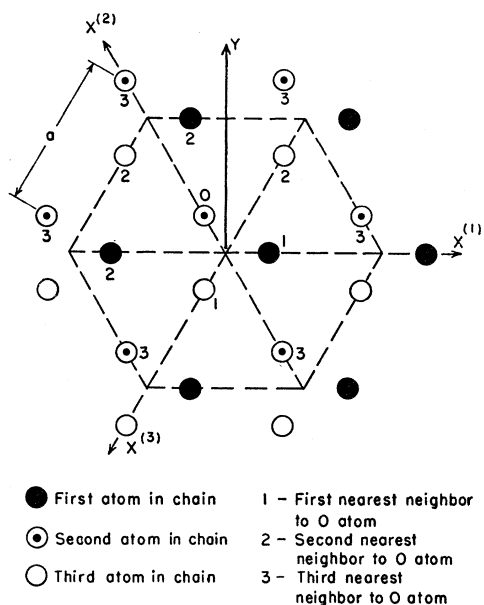


FIG. 1. Crystal structure of tellurium (trigonal screw axis along 0Z).

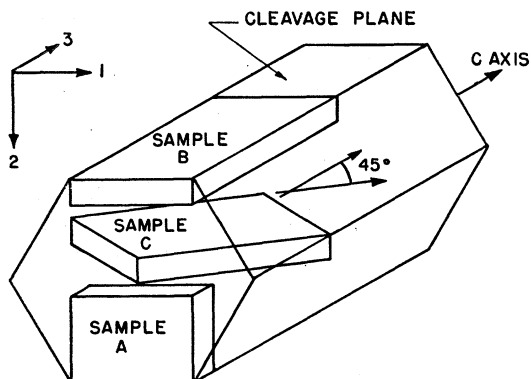


FIG. 2. Orientation of samples with respect to crystal axes.

* This research was supported in part by the U. S. Air Force Office of Scientific Research.

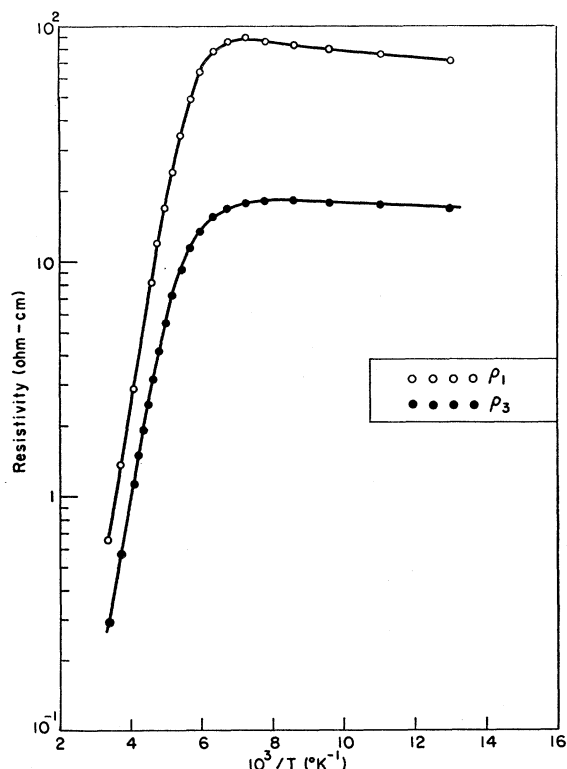


FIG. 3. Resistivity as a function of temperature parallel and perpendicular to the c axis.

¹ J. S. Blakemore, D. Long, K. C. Nomura, and A. Nussbaum, *Progress in Semiconductors*, Vol. 6 (to be published).

² T. J. Davies, *J. Appl. Phys.* 28, 1217 (1957).

³ H. Roth, *J. Phys. Chem. Solids* 8, 525 (1959).

coefficients will be found in an unpublished report.⁴ The values of all the coefficients at 77° and 300°K are given by Roth,³ and values at 4.2°K are given by Nussbaum and Long.⁵ In this paper we shall report the behavior over the temperature range 77°–300°K of all twelve of the galvanomagnetic coefficients and also show the effect of pressure on one of the two Hall coefficients over the temperature range encompassing the two reversals in sign. Finally, we shall postulate a band structure which correlates these results, plus those of other experimenters, with the symmetry properties of the lattice.

EXPERIMENTAL RESULTS

Tellurium crystals are very sensitive to mechanical handling and dislocations can be generated very easily.⁶ Preparation of the samples was accomplished by cleavage of 10 $\bar{1}0$ faces at 77°K, followed by a chemical polish to remove surface damage, as described by Blakemore *et al.*⁷ This technique also eliminates difficulties with the low-resistance surface layer reported by Caldwell and Fan.⁸ Figure 2 shows the orientation of the three samples used and also shows how they may be obtained

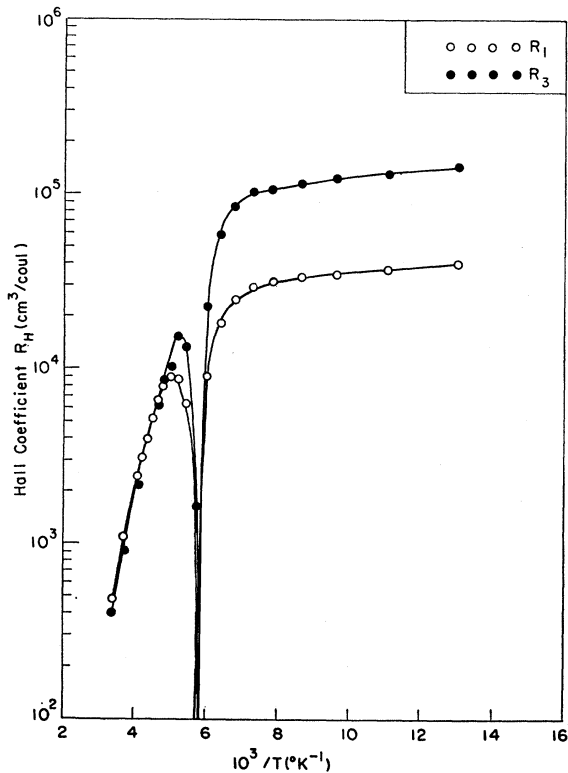


Fig. 4. Hall coefficients as a function of temperature.

⁴ H. Roth, General Atomic Laboratory Report GA-791, 1959 (unpublished).

⁵ A. Nussbaum and D. Long, Czech. J. Phys. (to be published).

⁶ R. J. Stokes and T. L. Johnston, Acta Met. (to be published).

⁷ J. S. Blakemore, J. W. Schultz, and K. C. Nomura, J. Appl. Phys. 31, 2226 (1960).

⁸ R. S. Caldwell and H. Y. Fan, Phys. Rev. 114, 664 (1959).

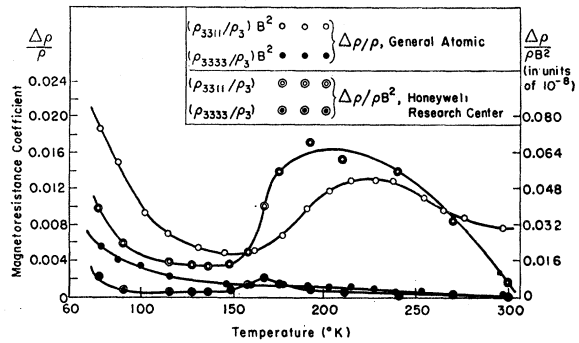


Fig. 5. Magneto-resistance coefficients ρ_{3311} and ρ_{3333} as a function of temperature.

from adjacent regions in the crystal by cleaving once to obtain sample *A* and then cleaving again to obtain samples *B* and *C*.

The galvanomagnetic tensor in an anisotropic semiconductor like tellurium can be defined in terms of the current-density *J*, the electric field *E*, and the magnetic field *B* as follows

$$J_p = \sum_{q,r,s=1}^3 [\sigma_{pq}E_q + \sigma_{pqr}E_qB_r + \sigma_{pqrs}E_qB_rB_s], \quad (1)$$

where σ_{pq} , σ_{pqr} , and σ_{pqrs} are the conductivity, Hall coefficient, and magnetoconductivity components, respectively. Inverting (1), the corresponding expression for the magneto-resistivity elements ρ_{ij} , ρ_{ijk} , and ρ_{ijkl} may be obtained. Using symmetry arguments, Roth⁴ has shown that the following twelve elements are non-vanishing: ρ_1 , ρ_3 , R_1 , R_3 , ρ_{1111} , ρ_{1133} , ρ_{1122} , ρ_{3333} , ρ_{3311} , ρ_{1313} , ρ_{1123} , and ρ_{2311} , where $\rho_1 = \rho_{11} = \rho_{22}$, $\rho_3 = \rho_{33}$, $R_1 = R_{231}$, and $R_3 = R_{123}$. Figures 3 through 9 show the dependence of these parameters on temperature in the range 77°–300°K. In addition, Fig. 5 shows the corresponding curve taken from Roth's paper³ and Fig. 7 shows the curve taken from his report.⁴ Roth's data were plotted in the form of $\Delta\rho/\rho$ or $(\rho_{ijij}/\rho_i)B^2$, whereas ours are given as $\Delta\rho/\rho B^2$ or ρ_{ijij}/ρ_i . The reason for incorporating the magnetic field strength into our data comes from the fact that it was necessary to adjust *B* at

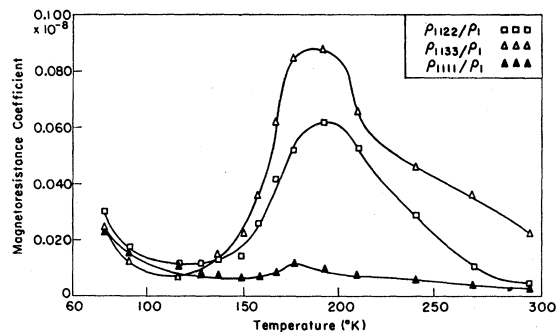


Fig. 6. Magneto-resistance coefficients ρ_{1111} , ρ_{1122} , and ρ_{1133} as a function of temperature.

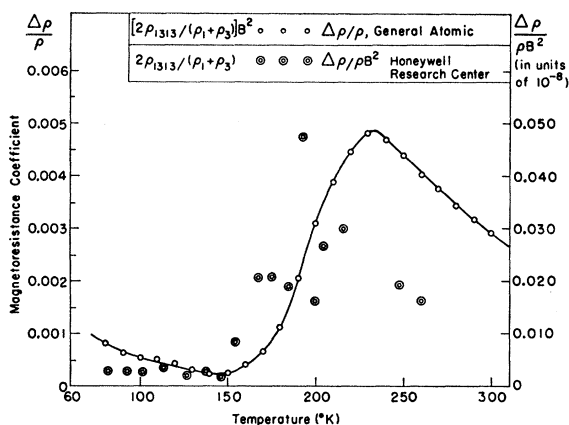


FIG. 7. Magnetoresistance coefficient ρ_{1313} as a function of temperature.

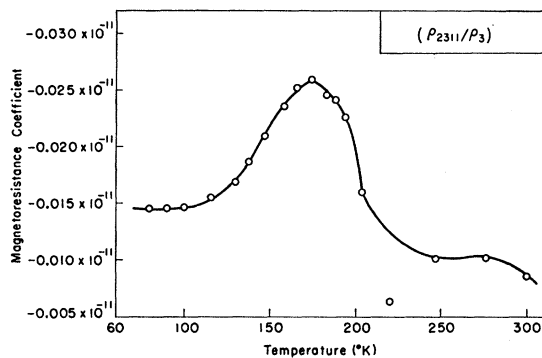


FIG. 8. Magnetoresistance coefficient ρ_{2311} as a function of temperature.

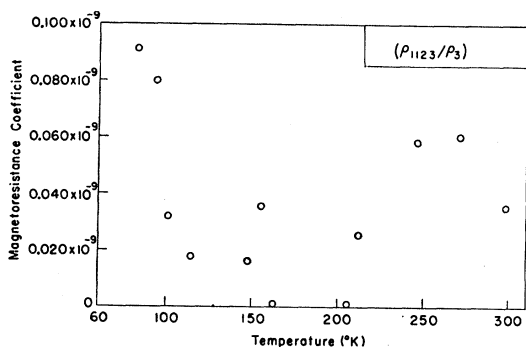


FIG. 9. Magnetoresistance coefficient ρ_{1123} as a function of temperature.

times during a run in order to hold the change in resistance to 1% or less of the zero-field value, thus ensuring that we were in the low-field region. Since Roth used a constant field of 5000 gauss, we can directly compare the shapes of the two sets of curves and we have adjusted the ordinates to make both sets fit vertical scales of the same size. The behavior of ρ_1 , ρ_3 , R_1 , R_3 , ρ_{1111} , ρ_{1122} , ρ_{1133} , ρ_{3333} , and ρ_{3311} were all very similar to Roth's, although the absolute values are not the same,

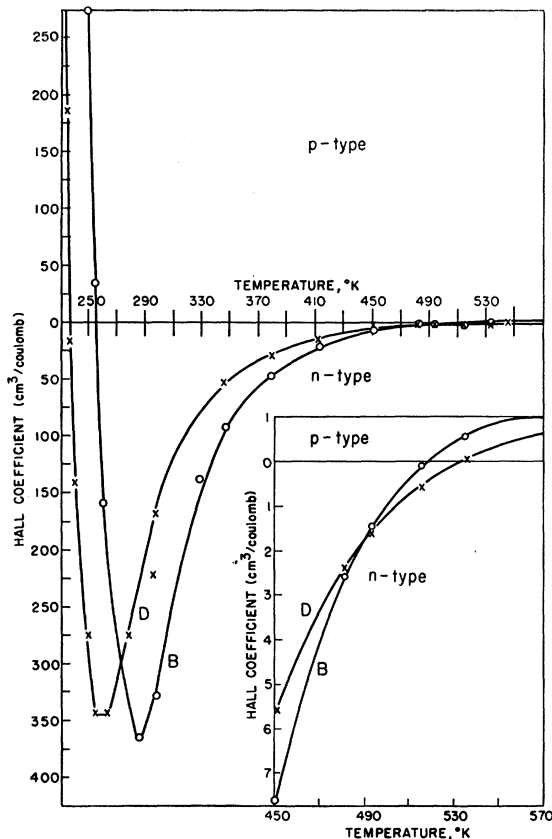


FIG. 10. Hall coefficient R_1 as a function of temperature and pressure. Curve *B*: atmospheric pressure; curve *D*: 2000 atm pressure.

and we have previously found⁵ this situation to exist even for samples cut from adjacent regions in the same crystal. For the coefficient ρ_{1313} , which cannot be measured directly but must be calculated from the small difference in two large numbers, we found that we could not reproduce the smooth curve of Roth, even though the temperature of the sample was regulated by using a heater in the liquid nitrogen with its current regulated by an automatic controller. Table I summarizes the values of the coefficients obtained at 77°K by Roth and by us, and at 4.2°K for a previous run in this laboratory, where the data in the last two columns of the table refer to the same set of samples. The second column of the table shows which sample of Fig. 2 is used to obtain each coefficient, and instructions for calculating the coefficients from the experimental data are given in detail in Roth's report.⁴

In addition to the results just presented, one further piece of information we shall use is the behavior of the Hall coefficient R_1 as a function of both temperature and pressure. It is known that the Hall coefficient in tellurium shows an anomalous double reversal in sign,⁹ and the effect of pressure on the upper reversal was pre-

⁹ P. I. Wold, Phys. Rev. 7, 169 (1916).

TABLE I. Galvanomagnetic coefficients of Te at 77°K and 4.2°K.

Coefficient	Sample type	Roth, ³ 77°K (5000 gauss)	Nussbaum and Long, ⁵ 4.2°K (1000 gauss)	Nussbaum and Hager, 77°K (~3000 gauss)
ρ_1 (ohm-cm)	A	52	22	71
ρ_3 (ohm-cm)	B	16	6	17
R_1 (cm ³ /coul)	B	2.6×10^4	13.5×10^4	4.0×10^4
R_3 (cm ³ /coul)	A	7.0×10^4	13×10^4	14.0×10^4
ρ_{1111}/ρ_1 (gauss ⁻²)	A	7.2×10^{-10}	6.5×10^{-8}	2.3×10^{-10}
ρ_{1133}/ρ_1 (gauss ⁻²)	A	8.7×10^{-10}	5.2×10^{-8}	3.0×10^{-10}
ρ_{1122}/ρ_1 (gauss ⁻²)	A	12×10^{-10}	9.5×10^{-8}	2.4×10^{-10}
ρ_{3333}/ρ_3 (gauss ⁻²)	B	2.2×10^{-10}	3.8×10^{-8}	0.90×10^{-10}
ρ_{3311}/ρ_3 (gauss ⁻²)	B	7.2×10^{-10}	16.5×10^{-8}	3.9×10^{-10}
$2\rho_{1313}/(\rho_1 + \rho_3)$ (gauss ⁻²)	C	-0.35×10^{-10}	~0	-0.23×10^{-10}
ρ_{1123}/ρ_1 (gauss ⁻²)	A	-0.4×10^{-10}	~0	0.91×10^{-10}
ρ_{2311}/ρ_3 (gauss ⁻²)	B	~0	~0	-0.14×10^{-12}

viously reported by Nussbaum *et al.*¹⁰ In Fig. 10, we show an extension of the curves for one of the two samples in this reference down to the lower reversal temperature. It is seen that the effect of pressure is to decrease the lower reversal temperature, in agreement with the results of Nussbaum¹¹ on a tellurium +13% selenium alloy, and increase the upper reversal temperature, contradicting the previous results on the alloy.

DISCUSSION

A. Proposed Energy Band Structure

Energy band curves as a function of lattice spacing for tellurium have been proposed by Callen¹² and Gáspár.¹³ Callen used the approximation of replacing the tellurium space group D_3^4 by the tetragonal point group D_{4h} and Gáspár used the much simpler three-atom arrangement C_{2v} as the basis of his arguments. Using tight-binding calculations, E vs k curves were given by Reitz¹⁴ and Asendorf¹⁵ which show extrema in the curves at the center and ends of the Brillouin zone. Herman¹⁶ has given curves for selenium for the empty lattice and nearly-empty lattice approximations which disagree somewhat with Reitz and Asendorf. We shall extend Herman's work to tellurium, and use the resulting pictures of the nearly empty lattice-band to interpret our data.

The symmetry operations for the tellurium lattice, as can be seen from Fig. 1, are as follows:

- (1) E , the identity.
- (2) (a) C_3 , a 120° rotation ρ_3 about the z axis followed by a translation of $c/3$, where c is the lattice constant along the OZ direction. We use the notation: $c_3 = (\rho_3 | c/3)$.
- (b) C_3^2 .

¹⁰ A. Nussbaum, J. Myers, and D. Long, Phys. Rev. Letters 2, 6 (1959).

¹¹ A. Nussbaum, Phys. Rev. 94, 337 (1954).

¹² H. B. Callen, J. Chem. Phys. 22, 518 (1954).

¹³ R. Gáspár, Acta. Phys. Acad. Sci. Hung. 7, 289 and 313 (1956).

¹⁴ J. R. Reitz, Phys. Rev. 105, 1233 (1957).

¹⁵ R. H. Asendorf, Ph.D. thesis, University of Pennsylvania, 1956 (unpublished).

¹⁶ F. Herman, Revs. Modern Phys. 30, 102 (1958).

(3) $C_2^{(1)}, C_2^{(2)}, C_2^{(3)}$: 180° rotations $\rho^{(1)}, \rho^{(2)}, \rho^{(3)}$ about the axes $X^{(1)}, X^{(2)}, X^{(3)}$, followed by translations as follows:

$$C_2^{(1)} = (\rho_2^{(1)} | c/3), \quad C_2^{(2)} = (\rho_2^{(2)} | 0), \quad C_3^{(3)} = (\rho_2^{(3)} | 2c/3).$$

We now propose to consider the appropriate symmetry operations along the two directions Δ and Σ in the Brillouin zone, shown in Fig. 11. The character tables are taken from Firsov¹⁷ and Asendorf,¹⁸ and we will follow the method of Jones¹⁹ for obtaining the compatibility relations (with the correction that the character table along the Δ axis must include the phase-factors).

For reasons of efficiency, let us consider first the symmetry operations associated with point $A(0,0,\pi/c)$ at the top of the Brillouin zone. A Bloch function

$$\psi_k(z) = e^{ikz} u_k(z) = e^{i\pi z/c} u_k(z) \quad (2)$$

at this point has an additional symmetry operation T , a displacement of c , associated with it, since $\psi_k(z)$ becomes $-\psi_k(z)$ when z becomes $z+c$. In addition,

$$T^2 = E,$$

as has been shown by Jones¹⁹ or Blakemore *et al.*¹ Combining T with the six operations above gives a closed group of twelve operations and six classes whose multiplication table will be found in Blakemore *et al.*¹ The associated character table is then given by Table II. The lower three irreducible representations A_1, A_2, A_3 belong only to functions associated with point A . For the point $\Gamma(0,0,0)$, the function $\psi_k(z)$ in (2), above, reduces

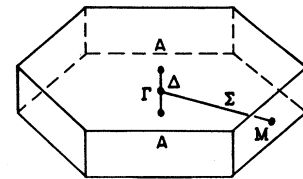


FIG. 11. Brillouin zone for tellurium.

¹⁷ Iu. A. Firsov, Soviet Phys.—JETP 5, 1101 (1957).

¹⁸ R. H. Asendorf, J. Chem. Phys. 27, 11 (1957).

¹⁹ H. Jones, *The Theory of Brillouin Zones and Electronic States in Crystals* (North-Holland Publishing Company, Amsterdam, 1960).

TABLE II. Character table for the points A and Γ .
(For the point Γ , the operation T is deleted.)

	E	C_3 TC_3^2	$C_2^{(1)}$ $TC_2^{(2)}$ $TC_3^{(3)}$	T	TC_3 C_3^2	$TC_2^{(1)}$ $C_2^{(2)}$ $C_3^{(3)}$
Γ_1	1	1	1	1	1	1
Γ_2	1	1	-1	1	1	-1
Γ_3	2	-1	0	2	-1	0
A_1	1	-1	1	-1	1	-1
A_2	1	-1	-1	-1	1	1
A_3	2	1	0	-2	-1	0

TABLE III. Character table for the point M and the axis Σ .

	E	$C_2^{(2)}$
Σ_1-M_1	1	1
Σ_2-M_2	1	-1

to $\psi_0(z)=u_0(z)$, which has the symmetry of the point group D_3 , and the operation T is equivalent to E . Hence, the character table for Γ is contained in the upper left-hand corner of the table for A . Table III shows the irreducible representations for the point M and the axis Σ , which we arbitrarily choose as being associated with the twofold rotation $C_2^{(2)}$. For the Δ axis, we must include the translational part $e^{ik_z t}$ of the character, as shown by Koster.²⁰ These phase-factors are combined with the characters of the point group C_3 to get Table IV. The compatibility relations are then obtained, according to Jones,¹⁹ by matching characters or sums of characters, as we proceed from Γ to A or Γ to M . These relations are given in Table V, and they differ from those of Asendorf¹⁸ due to the sign in the translational part of the characters. The relations along the Δ axis need a little bit of explanation. At Γ , the quantity δ in

TABLE IV. Character table for the Δ axis. $\omega=e^{2\pi i/3}$; $\delta=e^{ik_z t}$.

	E	C_3	C_3^2
Δ_1	1	δ	δ^2
Δ_2	1	$\omega\delta$	$\omega\delta^2$
Δ_3	1	$\omega^2\delta$	$\omega^2\delta^2$

TABLE V. Compatibility relations for Δ and Σ axes.

$\Gamma_1 \rightarrow \Sigma_1 \rightarrow M_1$	
$\Gamma_2 \rightarrow \Sigma_2 \rightarrow M_2$	
$\Gamma_3 \rightarrow \Sigma_1 + \Sigma_2$	
$\Gamma_1 \rightarrow \Delta_1,$	$A_1 \rightarrow \Delta_2$
$\Gamma_2 \rightarrow \Delta_1,$	$A_2 \rightarrow \Delta_2$
$\Gamma_3 \rightarrow \Delta_2 + \Delta_3,$	$A_3 \rightarrow \Delta_1 + \Delta_3$

²⁰ G. F. Koster, in *Solid-State Physics*, edited by F. Seitz and D. Turnbull (Academic Press, Inc., New York, 1957), Vol. 5.

Table IV becomes unity. Then $\omega + \omega^2 = \omega^2 + \omega = -1$, so that $\Gamma_3 \rightarrow \Delta_2 + \Delta_3$. At A , δ becomes $e^{i(\pi/c)(c/3)} = e^{i2\pi/6}$, and the character table is then

	E	C_3	C_3^2
Δ_1	1	$e^{2\pi i/6}$	$e^{2\pi i/3}$
Δ_2	1	$e^{2\pi i/2}$	$e^{4\pi i/3}$
Δ_3	1	$e^{5\pi i/6}$	$e^{2\pi i}$

The compatibility relations are then readily obtained.

Jones¹⁹ shows that the Bloch solution to the Schrödinger equation for the empty lattice approximation, $V(\mathbf{r})=0$, in tellurium is

$$\psi_{\mathbf{k}1} = \exp\left\{(2\pi i/a)[(\xi-l_1)x + (\eta - (l_1+l_2)/\sqrt{3})y + (a/c)(\zeta-l_3)z]\right\}, \quad (3)$$

and the energy levels are given by

$$E_{\mathbf{k}1} = (\xi-l_1)^2 + [\eta - (l_1+l_2)/\sqrt{3}]^2 + (a/c)^2(\zeta-l_3)^2, \quad (4)$$

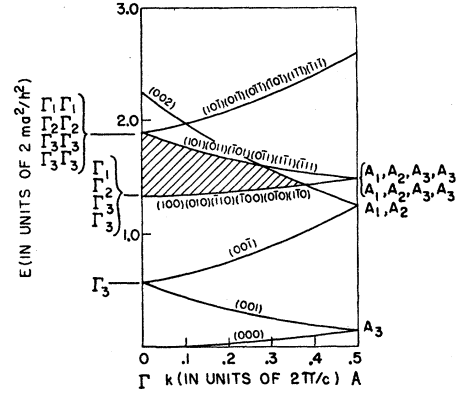
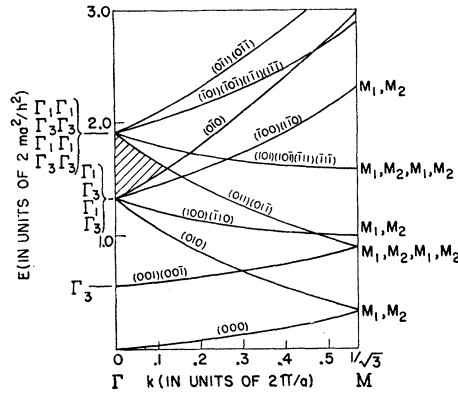
where (a/c) in tellurium is very close to 0.75, $\mathbf{k} = 2\pi(\xi/a, \eta/a, \zeta/a)$, and $\mathbf{l} = (l_1, l_2, l_3)$ where the $l = 0, \pm 1, \pm 2, \dots$. Using Eq. (4), E vs k curves are shown in Fig. 12 for the ΓA and ΓM axes. The integers (l_1, l_2, l_3) are marked on each curve and the number of sets of integers gives the degree of degeneracy. The position of the energy gap is determined by noting that the valence electrons in tellurium have the configurations $5s^2 5p^4$ and with three nonequivalent atoms, there will be eighteen valence electrons in the unit cell and nine valence functions. In comparing Fig. 12 with the corresponding diagram for selenium (Fig. 9 of Herman's review article¹⁶), it will be seen that there is a difference due to the difference in a/c ratios, 0.75 for tellurium and 0.88 for selenium. This leads to a band structure which differs from that for selenium (Herman's Fig. 10) and is shown in Fig. 13. This structure is based on the compatibility relations and on a determination of the associations between irreducible representations and the linear combinations of the functions of Eq. (3), using the method of Jones.¹⁹ Our structure also differs from that of Reitz¹⁴ and Asendorf,¹⁵ as discussed below.

B. The Many-Valley Model

In the band pictures of Fig. 13, we have shown the extrema as being located at intermediate positions on both the Σ and Δ axes. The symmetry of the lattice then requires a six-ellipsoid model for each band, and it is possible to obtain a semiquantitative understanding of some of our data by using the expressions developed for such a model by Drabble and Wolfe.²¹ The work of Drabble and Wolfe applies to bismuth telluride, which differs somewhat in its symmetry properties from tellurium. In Fig. 14, we show a comparison of the arrangement of the ellipsoids for these two materials.

²¹ J. R. Drabble and R. Wolfe, Proc. Phys. Soc. (London) **B69**, 1101 (1956).

FIG. 12. Empty lattice E vs k curves for tellurium.



For the same "tilt angle" θ , it has been shown²² that the relations given by Eqs. (25) of Drabble and Wolfe²¹ are also applicable to tellurium and they have already been used to establish the fact that the data for tellurium shows some consistency with the six-ellipsoid model at 4.2°K.⁵ In the range between 77° and 300°K, let us consider the following two typical relations, taken from Eq. (3) of Drabble and Wolfe,²¹

$$\rho_{1111}/\rho_1 = -\sigma_{1111}/\sigma_1, \tag{5}$$

$$\rho_{1133}/\rho_1 = -\sigma_{1133}/\sigma_1 - (\sigma_{123}/\sigma_1)^2. \tag{6}$$

The various ratios on the right-hand side of these equations predict temperature-dependences of the form T^n , where n is a small number. In the absence of a study of both pure and doped tellurium, it is not possible to analyze the data in a thorough fashion, since a number of temperature-dependent processes are occurring. For example, a preliminary study by Long and Kizilos²³ shows that the transition from lattice to impurity scattering in a number of samples of various purity

takes place in the range of 20°–30°K. However, it can be seen that Eq. (6) predicts that there should be a rise in the value of ρ_{1133}/ρ_1 as the Hall coefficient goes through zero, whereas ρ_{1111}/ρ_1 should be independent of this effect, and this prediction is in agreement with the curves of Fig. 6. Similar results are obtained by comparing the Drabble and Wolf formulas with the other magnetoresistance coefficients.

C. Effect of Pressure on the Band Structure

The band structure of Fig. 13 has been drawn to correspond with the fact that the energy gap of tellurium (0.33 eV) is considerably smaller than that of selenium (~2 eV). It is known²⁴ that the effect of pressure is to increase the lattice constant c and reduce the lattice constant a , thus making the a/c ratio more tellurium-

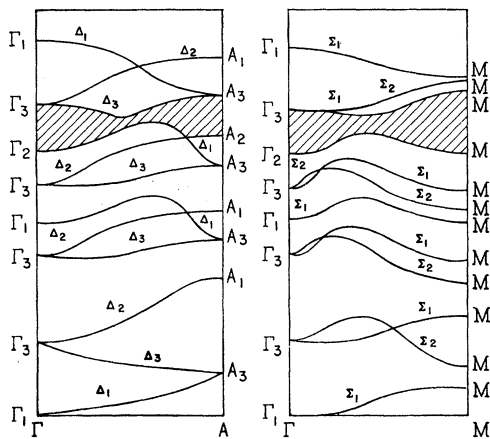


FIG. 13. Nearly-empty lattice E vs k curves for tellurium.

²² D. Long and A. Nussbaum, in Honeywell Research Center Quarterly Report, Air Force Office of Scientific Research, Project AF 49(638)-908, August 31, 1960 (unpublished).

²³ D. Long and B. Kizilos, see reference 22.

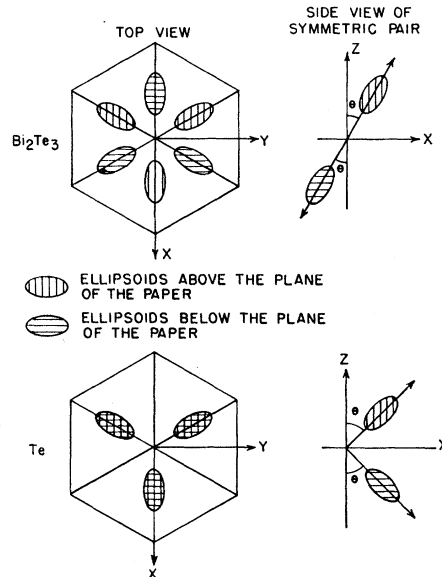


FIG. 14. Comparison of the arrangement of the ellipsoids in bismuth telluride and tellurium.

²⁴ D. Long, Phys. Rev. **101**, 1256 (1956).

like and less selenium-like. This effect is thus consistent with the pressure work of Long,²⁴ who found an 0.03-eV decrease in the gap of tellurium using the same pressure as that of Fig. 10, and similarly, Neuringer²⁵ found a decrease in the optical gap when pressure was applied. This accounts for the decrease in the lower reversal temperature with pressure. For the upper reversal, we have indicated a double valence band, and the activation of the light, higher-mobility holes from the lower-lying band can be the cause of the second reversal. The application of pressure, while it decreases the gap, can also cause a redistribution among the states in the two bands and cause the Hall coefficient to reverse at a higher temperature. The location of the extrema at the positions shown in the two parts of Fig. 13 disagrees with the tight-binding calculations, which predict the occurrence of the thermal gap at π/c . Further, we show a double valence band, rather than a degenerate one, and the separation of the two valence bands is schematically indicated as being large enough so that the light-hole band is not activated until the temperature approaches 300°K.

D. Optical Measurements

The optical absorption edge of tellurium was first shown by Loferski²⁶ to be dichroic. Moreover, his results (which covered only a limited range of absorption coefficient) seemed to indicate the absorption edges at appreciably different energies for the two polarizations $E\parallel C$, $E\perp C$. Much of the earlier theoretical work on the band structures, such as that of Callen, Gáspár, and

Reitz, has been preoccupied with devising selection rules which would explain this result. However, the more recent optical absorption data of Nomura and Blakemore^{27,28} covers a much wider range (from 0.01 cm^{-1} to 1000 cm^{-1}) and strongly indicates that the absorption edge is the same for both polarizations. The shape of the absorption coefficient vs energy curves are different for the two polarizations, as would be expected if one transition were allowed and the other nominally forbidden, yet both originate from the same point in the uppermost valence band of Fig. 13. In addition, Caldwell and Fan⁸ have already proposed the double valence band as an explanation for the 11-micron absorption which they observed. We can therefore state that the band structure proposed here is in accord with the optical properties of tellurium as they are now understood to exist.

ACKNOWLEDGMENTS

We should like to thank our colleagues on the Honeywell Research Center tellurium program—Dr. Donald Long, Dr. John Blakemore, Dr. Carl Nomura—for many helpful discussions and for permission to quote unpublished results. We should also like to express our appreciation to Dr. Frank Herman of the RCA Laboratories for a great deal of help on the subtle mysteries of group theory. Finally, we should like to acknowledge the constant technical and personal encouragement of Dr. Charles A. Domenicali.

²⁷ K. C. Nomura and J. S. Blakemore, in Honeywell Research Center Quarterly Report, Air Force Office of Scientific Research, Project AF 49(638)-908, March 1, 1961 (unpublished).

²⁸ K. C. Nomura and J. S. Blakemore, *Bull. Am. Phys. Soc.* **5**, 62 (1960).

²⁵ L. J. Neuringer, *Phys. Rev.* **113**, 1495 (1959).

²⁶ J. J. Loferski, *Phys. Rev.* **93**, 707 (1956).